



Cross-Modality Fusion Transformer for Multispectral Object Detection

Fang Qingyun, Han Dapeng, Wang Zhaokui**

School of Aerospace Engineering, Tsinghua University, Beijing, 100084 China

Article history:

Keyword: Cross-modality, feature fusion, multispectral object detection, Transformer

ABSTRACT

Multispectral image pairs can provide the combined information, making object detection applications more reliable and robust in the open world. To fully exploit the different modalities, we present a simple yet effective cross-modality feature fusion approach, named Cross-Modality Fusion Transformer (CFT) in this paper. Unlike prior CNNs-based works, guided by the Transformer scheme, our network learns long-range dependencies and integrates global contextual information in the feature extraction stage. More importantly, by leveraging the self attention of the Transformer, the network can naturally carry out simultaneous intra-modality and inter-modality fusion, and robustly capture the latent interactions between RGB and Thermal domains, thereby significantly improving the performance of multispectral object detection. Extensive experiments and ablation studies on multiple datasets demonstrate that our approach is effective and achieves state-of-the-art detection performance. Our code and models are available at <https://github.com/DocF/multispectral-object-detection>.

© 2021 Elsevier Ltd. All rights reserved.

1. Introduction

In real-world object detection applications, the environment is often open and dynamic, requiring models and algorithms to deal with the challenges caused by openness, such as rain, fog, occlusions, poor lighting, low resolution, etc. It is difficult for an algorithm that uses only visible-band sensor data to achieve high accuracy under these conditions. Hence, the multispectral imaging technology is gradually being adopted, given its ability to provide the combined information coming from multispectral cameras e.g., visible and thermal. And by fusing the complementary of different modalities, the perceptibility, reliability, and robustness of detection algorithms can be further improved.

Recent advances in convolutional neural networks (CNNs), more specifically, two-stream CNN-based detectors, have encouraged detection performance in the field of multispectral object detection[1–11]. In addition, some challenging multispectral datasets, e.g. FLIR[12], LLVIP[13], VEDAI[14], have also driven the continuous development of this field.

Figure 1 shows some examples to illustrate the advantages of

multispectral images over visible-only or thermal-only images under different conditions. However, the exploitation of multispectral data will raise some new questions: How to integrate the representations to fully make use of the inherent complementary between different modalities? And how to design an effective cross-modality fusion mechanism for maximum performance gain?

In the prior works, no matter how to design the modal fusion mechanism, they are all mostly based on deep convolutional neural networks[1, 3, 5, 7, 8]. There is considerable literature that has proven that CNNs can have strong representation learning capabilities within a single intra-modal reasoning [15–20], especially for visual modality. However, it is non-trivial to extend them to cross-modality fusion or modality interaction to fully exploit the inherent complementary. The convolution operator of CNNs can be regarded as a non-fully connected graph with each spatial position in the feature maps as a node. Since the convolution operator has a non-global receptive field, the information is only fused in a local area. In contrast, the self attention operator of Transformer [21] can be regarded as a fully connected graph, so it can learn long-range dependencies and its receptive field can be global. For the above considerations, we propose a novel and effective multispectral fusion approach, which is called *Cross-Modality Fusion Transformer* (CFT), to integrate global contextual information of different modalities in the feature extraction backbone. And to the best of our

**Corresponding author

e-mail: fqy17@mails.tsinghua.edu.cn (Fang Qingyun),
dphan@mail.tsinghua.edu.cn (Han Dapeng),
wangzk@tsinghua.edu.cn (Wang Zhaokui)



Fig. 1. Visible-infrared paired examples from LLVIP. The paired images in the first row are captured in nighttime traffic scenes. Compared with the visual image on the left, the thermal image on the right can capture the clearer contours of pedestrians under insufficient illumination conditions. Besides, the thermal image also captures pedestrians obscured by a pillar. The paired images in the second row are captured in daytime traffic scenes. During well-lit daytime, the visual image has more details, such as edges, textures, and colors, than thermal images. With these details, we can easily find the driver hidden in the motor tricycle, which is difficult to find in the thermal image. Zoom in to see details.

knowledge, this is the first work adopting the Transformer for multispectral object detection.

Contributions: (1) We introduce a new and powerful two-stream backbone that enhances one modality from another modality under the guidance of the Transformer scheme. (2) We propose a simple yet effective CFT module, and give theoretical insights into it, showing that the CFT module simultaneously fuses the intra-modality and inter-modality features. (3) Experimental results achieve the state-of-the-art performance on three public datasets, which confirm the effectiveness of the proposed approaches.

2. Relate work

Fusing the feature of two modalities is the core problem in multispectral object detection, which can be described as

$$\mathbf{F}_{Fused} = \mathcal{F}(\mathbf{F}_R, \mathbf{F}_T), \quad (1)$$

where \mathbf{F}_R denotes the RGB modality features and \mathbf{F}_T denotes the Thermal modality features. \mathbf{F}_{Fused} indicates the fused features, and $\mathcal{F}(\mathcal{X})$ is considered as the function of fusion. In the Eq. (1), multi-modality fusion can be studied in two aspects: input variable, i.e., input features, and fusion functions. Therefore, following the idea of Eq. (1), the previously published studies can be also divided into two categories, one focused on the input features (“macro” level), and the other focused on constructing the fusion functions (“micro” level).

Macro level. This type of paper is aimed to solve the problem of where to fuse, that is, which stage of the input features

to choose to fuse. Most of them always explore the best fusion stage by designing the macro network architectures. The first study of this type [22] investigates two deep fusion architectures (early fusion and late fusion) and analyzes their performance on multispectral data. To further explore the potential of deep models for multispectral pedestrian detection, Liu et al. [1] carefully design another two ConvNet fusion architectures (halfway fusion and score fusion), and demonstrate that the halfway fusion model achieved the best detection synergy. Since then, several subsequent work [3, 4, 7, 23] has illustrated that the halfway fusion is overwhelmingly outperforming than other three fusion architectures.

Mirco level. Besides the macro network architectures, the construction of fusion function is another point for complementary learning of modality interaction. Naturally, the most straightforward way is to utilize concatenation, element-wise addition, element-wise average/maximum, and element-wise cross product to direct fuse feature maps of RGB and Thermal modalities. Two variations of novel Gated Fusion Units (GFU) [24] are proposed in GFD-SSD to learn the combination of feature maps generated by the two SSD middle layers. Zhang et. al. [6] propose a novel cycle fuse-and-refine module to improve the multispectral feature fusion while taking into account the complementary/consistency balance of the features. Different from the prior methods, we suggest a Transformer-based scheme to carry out intra-modal and inter-modal information fusion with the help of self attention.

3. Proposed Method

Overview. To demonstrate the effectiveness of our proposed CFT fusion module, we extend the framework of YOLOv5, to enable multispectral object detection. To be precise, we re-design the YOLOv5 feature extraction network to become a two-stream backbone, and embedded the CFT modules to facilitate modal fusion and modal interaction, named as *Cross-Modality Fusion Backbone*. An illustration of our *Cross-Modality Fusion Backbone* and *Cross-Modality Fusion Transformer* is presented in Fig. 2.

Formulated details. Specifically, given the intermediate RGB convolution feature maps $\mathbf{F}_R \in \mathbb{R}^{C \times H \times W}$, and thermal convolution feature maps $\mathbf{F}_T \in \mathbb{R}^{C \times H \times W}$, the sentences $\mathbf{I}_R \in \mathbb{R}^{HW \times C}$ and $\mathbf{I}_T \in \mathbb{R}^{HW \times C}$ are obtained by flattening each feature map and permuting the order of the matrices. Second, we concatenate the sentences of each modality and add a learnable positional embedding, which is a trainable parameter of dimension $2HW \times C$, to get the input sentences $\mathbf{I} \in \mathbb{R}^{2HW \times C}$ of the Transformer. The positional embedding enables the model to discriminate spatial information between different tokens at train time. Third, the input sequence \mathbf{I} is projected onto three weight matrices to compute a set of queries, keys and values (\mathbf{Q} , \mathbf{K} and \mathbf{V}),

$$\mathbf{Q} = \mathbf{I}\mathbf{W}^Q, \quad (2)$$

$$\mathbf{K} = \mathbf{I}\mathbf{W}^K, \quad (3)$$

$$\mathbf{V} = \mathbf{I}\mathbf{W}^V, \quad (4)$$

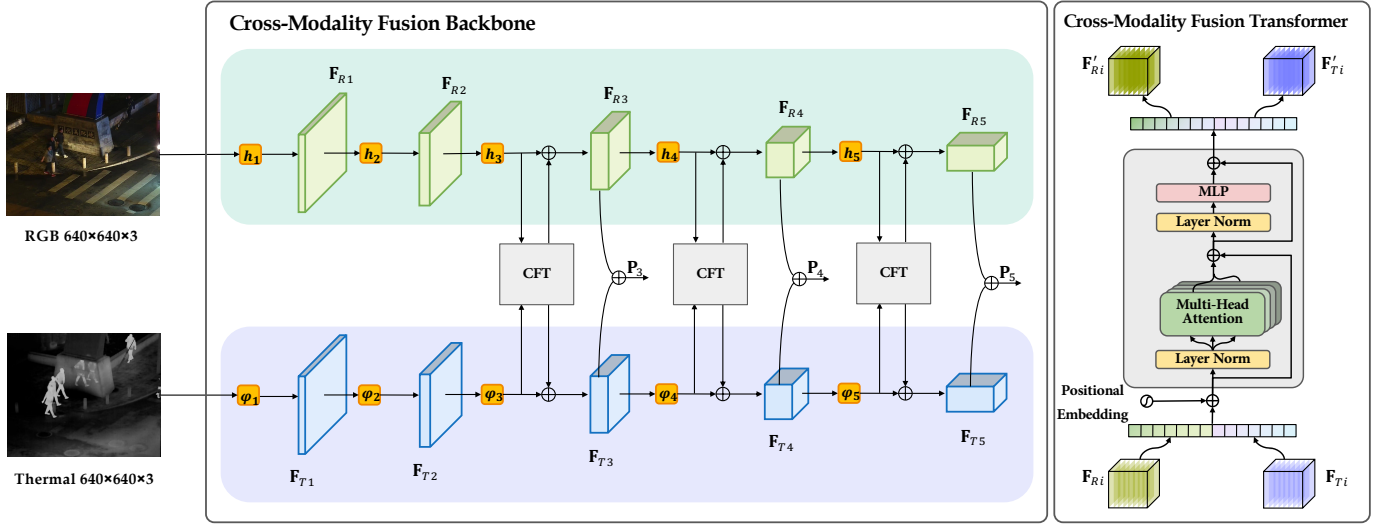


Fig. 2. Overview framework of Cross-Modality Fusion Backbone. The backbone consists of two parts: a two-stream feature extraction network and a Cross-Modality Fusion Transformer module. Among them, h_i and φ_i are the convolution modules of the RGB and Thermal branches, F_{Ri} and F_{Ti} are the feature maps of their respective modalities, and P_i represents the input of the feature pyramid.

where $\mathbf{W}^Q \in \mathbb{R}^{C \times D_Q}$, $\mathbf{W}^K \in \mathbb{R}^{C \times D_K}$ and $\mathbf{W}^V \in \mathbb{R}^{C \times D_V}$ are weight matrices. Moreover, D_Q , D_K and D_V are equal in our Transformer, i.e., $D_Q = D_K = D_V = C$. Fourth, the self attention layer uses the scaled dot products between \mathbf{Q} and \mathbf{K} to compute the attention weights and then multiply by the values to infer the refined output \mathbf{Z} ,

$$\mathbf{Z} = \text{Attention}(\mathbf{Q}, \mathbf{K}, \mathbf{V}) = \text{softmax}\left(\frac{\mathbf{Q}\mathbf{K}^T}{\sqrt{D_K}}\right)\mathbf{V}, \quad (5)$$

where $\frac{1}{\sqrt{D_K}}$ is a scaling factor for preventing the softmax function from converging to a region with extremely small gradients when the magnitude of dot products grow large. To encapsulate multiple complex relationships from different representation subspaces at different positions, the multi-head attention mechanism is adopted,

$$\begin{aligned} \mathbf{Z}' &= \text{MultiHead}(\mathbf{Q}, \mathbf{K}, \mathbf{V}) = \text{Concat}(\mathbf{Z}_1, \dots, \mathbf{Z}_h) \mathbf{W}^O, \\ \mathbf{Z}_i &= \text{Attention}(\mathbf{Q}\mathbf{W}_i^Q, \mathbf{K}\mathbf{W}_i^K, \mathbf{V}\mathbf{W}_i^V). \end{aligned} \quad (6)$$

The subscript h denotes the number of heads, and $\mathbf{W}^O \in \mathbb{R}^{h \times C \times C}$ denotes the projected matrix of $\text{Concat}(\mathbf{Z}_1, \dots, \mathbf{Z}_h)$. Then the Transformer uses a two-layer fully connected feed-forward network with a GELU [25] activation in between to calculate the output sequences \mathbf{O} , which are of the same shape as input sequences \mathbf{I} ,

$$\mathbf{O} = \text{MLP}(\mathbf{Z}'') + \mathbf{Z}'', \quad (7)$$

$$= \text{FC}_2(\text{GELU}(\text{FC}_1(\mathbf{Z}''))) + \mathbf{Z}'' \quad (8)$$

where $\mathbf{Z}'' = \mathbf{Z}' + \mathbf{I}$. Finally, exploiting the inverse operation of the first step, the output sentences \mathbf{O} are converted into the recalibration results \mathbf{F}'_R and \mathbf{F}'_T and add to the original modality branch as complementary information.

Implementation details. The parameter amount and computational complexity of a standard Transformer block can be

formalized as

$$\text{Params} \sim O(\text{Transformer}) = 4HWC + 8C^2, \quad (9)$$

$$\text{FLOPs} \sim \Omega(\text{Transformer}) = 12HWC^2 + 2(HW)^2C. \quad (10)$$

And a CFT module has 8 duplicate Transformer blocks, as shown in Fig. 2. In addition, since the dimension of the input sentences \mathbf{I} is $2HW \times C$, the actual expression of HW in the above Eq. (9) and (10) is $2HW$. Apart from the Parameters and FLOPs, the memory access also needs to be considered [26], especially when calculating the dot product of queries and keys, an intermediate matrix of $2HW \times 2HW$ dimensions will be generated. When the input picture size is 640×640 , after two downsamplings ($H = W = 160$), the elements of the matrix $\mathbf{Q}\mathbf{K}^T$ exceed 2.4G, which is unacceptable for ordinary computers.

For the sake of reducing expensive computation, our solution is to use a global average pooling that downsamples the feature maps to a low and fixed resolution of $H = W = 8$ before passing them to the Transformer block. And the output is upsampled by bilinear interpolation to the original resolution before being added to the original mode branch.

Why Transformer? The main idea behind our module is leveraging the self attention mechanism to learn the binary relationship of RGB and Thermal modalities, more precisely, leveraging the correlation matrix to weight each position of the input feature maps. It can be formulated as:

$$\alpha = \text{softmax}\left(\frac{\mathbf{Q}\mathbf{K}^T}{\sqrt{D_K}}\right) = \begin{matrix} & \begin{matrix} C_1 & \cdots & C_{HW} & C_{HW+1} & \cdots & C_{2HW} \end{matrix} \\ \begin{matrix} L_1 \\ \vdots \\ L_{HW} \\ L_{HW+1} \\ \vdots \\ L_{2HW} \end{matrix} & \left(\begin{array}{cccc|cccc} \alpha_{1,1} & \alpha_{1,2} & \cdots & \alpha_{1,HW} & \alpha_{1,HW+1} & \alpha_{1,HW+2} & \cdots & \alpha_{1,2HW} \\ \alpha_{2,1} & \alpha_{2,2} & \cdots & \alpha_{2,HW} & \alpha_{2,HW+1} & \alpha_{2,HW+2} & \cdots & \alpha_{2,2HW} \\ \vdots & \vdots & \ddots & \vdots & \vdots & \vdots & \ddots & \vdots \\ \alpha_{HW,1} & \alpha_{HW,2} & \cdots & \alpha_{HW,HW} & \alpha_{HW,HW+1} & \alpha_{HW,HW+2} & \cdots & \alpha_{HW,2HW} \\ \alpha_{HW+1,1} & \alpha_{HW+1,2} & \cdots & \alpha_{HW+1,HW} & \alpha_{HW+1,HW+1} & \alpha_{HW+1,HW+2} & \cdots & \alpha_{HW+1,2HW} \\ \alpha_{HW+2,1} & \alpha_{HW+2,2} & \cdots & \alpha_{HW+2,HW} & \alpha_{HW+2,HW+1} & \alpha_{HW+2,HW+2} & \cdots & \alpha_{HW+2,2HW} \\ \vdots & \vdots & \ddots & \vdots & \vdots & \vdots & \ddots & \vdots \\ \alpha_{2HW,1} & \alpha_{2HW,2} & \cdots & \alpha_{2HW,HW} & \alpha_{2HW,HW+1} & \alpha_{2HW,HW+2} & \cdots & \alpha_{2HW,2HW} \end{array} \right) \end{matrix}, \quad (11)$$

where $\alpha_{i,j}$ represents the correlation between the i -th position and the j -th position on the feature maps. According to the Eq. (11), four matrix blocks can be inferred naturally, when calculating the correlation matrix α . Two of them are intra-modality correlation matrix blocks (RGB and Thermal), and the other two are inter-modality correlation matrix blocks, as illustrated in Fig. 3.

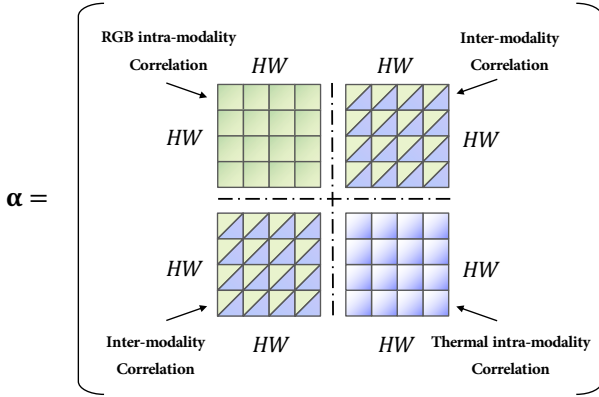


Fig. 3. Illustration of the correlation matrix α .

Hence, with the help of Transformer, we don’t need to carefully design the modal fusion module. We just only needs to simply splice the multi-modal features into a sequence, and then the Transformer can automatically perform simultaneous intra-modality and inter-modality information fusion and robustly capture the latent interactions between RGB and Thermal domains.

4. Experiment

4.1. Datas

FILP. The FLIR ADAS dataset [12] is a challenging multi-spectral object detection dataset which includes day and night scenes. There are a lot of unaligned image pairs in the original data set, which makes network training difficult. Therefore, an “aligned” version [6] is recently released that manually removes unaligned visible-thermal image pairs. This new dataset contains 5,142 well-aligned multispectral image pairs, of which 4,129 pairs are used for training and 1,013 pairs are used for

testing and cover three object categories: “person”, “car” and “bicycle”.

LLVIP. LLVIP [13] is a very recently released visible-infrared paired pedestrians dataset for low-light vision. This dataset contains 33672 images, or 16836 pairs, most of which were taken at very dark scenes, and all of the images are strictly Spatio-temporal aligned.

VEDAI. In addition to the above two ground-view datasets, we also test our method on VEDAI [14] which is a multispectral aerial imagery dataset for vehicle detection. The dataset contains nine vehicle classes for a total of more than 3700 annotated targets in more than 1200 images in each resolution (1024×1024 and 512×512). Both RGB and NIR modalities are available for each image.

4.2. Training Details

In these experiments, YOLOv5 is chosen as our base detector. By adding an additional branch for the extraction of thermal features, it is transformed into a two-stream convolutional neural network, as illustrated in Fig. 2. We use SGD optimizer with an initial learning rate of $1e-2$, a momentum of 0.937, and a weight decay of 0.0005. As for data augmentation, we use the Mosaic method which mixes four training images in one image.

4.3. Ablation Study

All models are evaluated with three usual object detection metrics introduced with MS-COCO: mAP50, mAP75, and mAP. The best records and the improvements are marked in bold and \uparrow , respectively. In Table 1, we compare the detection performance with and without CFT on different datasets (FLIR, LLVIP, and VEDAI). And the results confirm that our CFT has general significance for improving the performance of multispectral object detection.

Table 1. Ablation Experiments on Three Datasets

Dataset	CFT	mAP50	mAP75	mAP
FLIR		73.0	32.0	37.4
	✓	77.7 ($\uparrow 4.7$)	34.8 ($\uparrow 2.8$)	40.0 ($\uparrow 2.6$)
LLVIP		95.8	71.4	62.3
	✓	97.5 ($\uparrow 1.7$)	72.9 ($\uparrow 1.5$)	63.6 ($\uparrow 1.3$)
VEDAI		79.7	47.7	46.8
	✓	85.3 ($\uparrow 5.6$)	65.9 ($\uparrow 8.2$)	56.0 ($\uparrow 9.2$)

Additionally, to more intuitively evaluate the detection results, we qualitatively compare our CFT with baselines on FLIR, LLVIP, and VEDAI datasets, in Fig. 4, Fig. 5 and Fig. 6, respectively. Visually, even for densely obscured objects, our CFT method can still detect all objects, while the baselines have multiple false positives or false negatives, i.e., wrong detection.



Fig. 4. Qualitative comparison of multispectral object detection results in the FLIR ADAS dataset. The first column is the color image and the second is the thermal image. The first row, the second row, and the last row are ground truth, detection results of the baseline, and detection results of our method (CFT), respectively. Note that red inverted triangles indicate FNs. Zoom in to see details.

4.4. Comparison with State-of-the-art Methods

On FLIR. Tabel 2 reports the experimental results of our approach and other methods for comparison. It can be observed that our CFT achieves state-of-the-art performance on this dataset. Furthermore, it wins with an overwhelming advantage, and the gap between CFT and others is at least 4.8%, and up to 6.5% on mAP50. Even compared to the latest GAFF [7], our method outperforms 4.8%, 1.9%, and 2.5% on mAP50, mAP75, and mAP respectively, which is a significant improvement on this dataset.

On LLVIP. Table 3 presents the detection results of CFT and other mono-modality networks, especially YOLOv5 which is the basis of our algorithm, on the LLVIP dataset. What stands out in the table (below) is that a more accurate detection (mAP50:97.5, mAP75:72.9, mAP:63.6) can be pushed by fusing the complementary features of different modalities based on the Transformer.

On VEDAI. As mentioned before, the multispectral aerial imagery dataset VEDAI is used in this experiment. Again,



Fig. 5. Qualitative comparison of multispectral object detection results in the LLVIP dataset. The arrangement of this figure is the same as the Fig. 4. Note that red inverted triangles indicate FNs. Zoom in to see details.

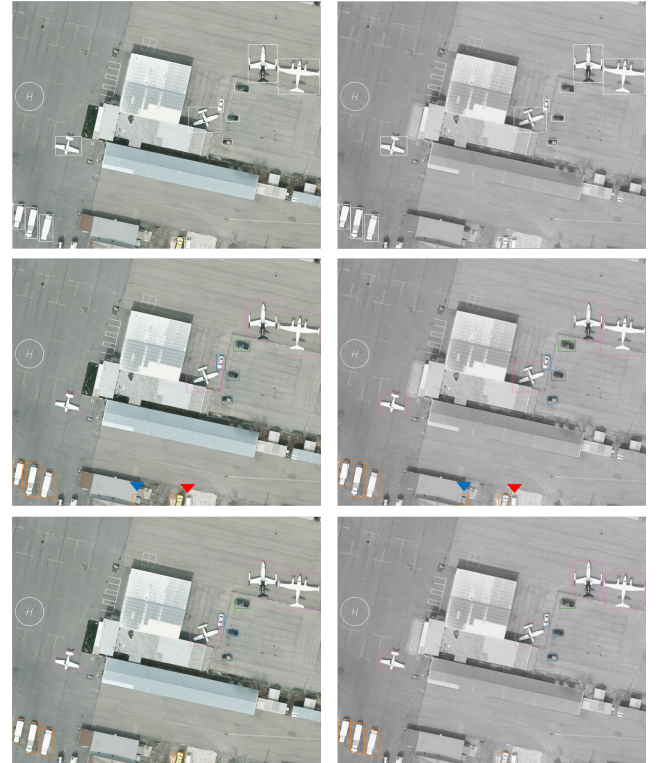


Fig. 6. Qualitative comparison of multispectral object detection results in the VEDAI dataset. The arrangement of this figure is the same as the Fig. 4. Note that red inverted triangles indicate FNs, and blue inverted triangles show FPs. Zoom in to see details.

Table 2. Comparison on FLIR Dataset

Model	Data	Backbone	mAP50	mAP75	mAP
mono-modality networks					
YOLOv5	RGB	CSPDarknet53	67.8	25.9	31.8
YOLOv5	IR	CSPDarknet53	73.9	35.7	39.5
multi-modality networks					
halfway fusion [6]	RGB+IR	VGG16	71.2	-	-
CFR_3 [6]	RGB+IR	VGG16	72.4	-	-
GAFF [7]	RGB+IR	ResNet18	72.9	32.9	37.5
GAFF [7]	RGB+IR	VGG16	72.7	30.9	37.3
Baseline(Ours)	RGB+IR	CSPDarknet53	73.0	32.0	37.4
CFT(Ours)	RGB+IR	CFB	77.7	34.8	40.0

Table 3. Comparison on LLVIP Dataset

Model	Data	Backbone	mAP50	mAP75	mAP
mono-modality networks					
YOLOv3 [13]	RGB	Darknet53	85.9	37.9	43.3
YOLOv3 [13]	IR	Darknet53	89.7	53.4	52.8
YOLOv5 [13]	RGB	CSPDarknet53	90.8	51.9	50.0
YOLOv5 [13]	IR	CSPDarknet53	94.6	72.2	61.9
multi-modality networks					
Baseline(Ours)	RGB+IR	CSPDarknet53	95.8	71.4	62.3
CFT(Ours)	RGB+IR	CFB	97.5	72.9	63.6

we can observe from Table 4 that our method brings very impressive gains for all the considered evaluation metrics (mAP50: $\uparrow 9.3$, mAP: $\uparrow 10.0$).

5. Conclusion

In this work, we propose a novel transformer-based fusion approach, named Cross-Modality Fusion Transformer (CFT), to enhance the representation capability of two-stream CNNs in multispectral object detection. More specifically, the CFT modules are densely inserted in the backbone to integrate features, so the inherent complementary between different modalities can be fully exploited. Moreover, we derive the process of how the CFT module fuses the multi-modality feature maps from the formula and implementation view. Extensive experiments demonstrate that our proposed method can achieve the state-of-the-art performance. Given that our approach is simple yet effective, it may do a favor to other computer vision fields such as RGB-LiDAR, RGB-D, stereo image SR tasks, etc.

6. Acknowledgement

This work was supported by the National Natural Science Foundation of China under Grant No.U20B2056 and No.11872034.

References

- [1] J. Liu, S. Zhang, S. Wang, D. N. Metaxas, Multispectral deep neural networks for pedestrian detection, in: R. C. Wilson, E. R. Hancock, W. A. P. Smith (Eds.), *Proceedings of the British Machine Vision Conference 2016, BMVC 2016, York, UK, September 19-22, 2016*.
- [2] K. Park, S. Kim, K. Sohn, Unified multi-spectral pedestrian detection based on probabilistic fusion networks, *Pattern Recognition* 80 (2018) 143–155. doi:10.1016/j.patcog.2018.03.007.
- [3] C. Li, D. Song, R. Tong, M. Tang, Multispectral pedestrian detection via simultaneous detection and segmentation, in: *British Machine Vision Conference 2018, BMVC 2018, Newcastle, UK, September 3-6, 2018*, 2018, p. 225.
- [4] C. Li, D. Song, R. Tong, M. Tang, Illumination-aware faster R-CNN for robust multispectral pedestrian detection, *Pattern Recognition* 85 (2019) 161–171. doi:10.1016/j.patcog.2018.08.005.
- [5] L. Zhang, Z. Liu, S. Zhang, X. Yang, H. Qiao, K. Huang, A. Hussain, Cross-modality interactive attention network for multispectral pedestrian detection, *Information Fusion* 50 (2019) 20–29. doi:10.1016/j.inffus.2018.09.015.
- [6] H. Zhang, É. Fromont, S. Lefèvre, B. Avignon, Multispectral fusion for object detection with cyclic fuse-and-refine blocks, in: *IEEE International Conference on Image Processing, ICIP 2020, Abu Dhabi, United Arab Emirates, October 25-28, 2020*, pp. 276–280. doi:10.1109/ICIP40778.2020.9191080.
- [7] H. Zhang, É. Fromont, S. Lefèvre, B. Avignon, Guided attentive feature fusion for multispectral pedestrian detection, in: *IEEE Winter Conference on Applications of Computer Vision, WACV 2021, Waikoloa, HI, USA, January 3-8, 2021*, pp. 72–80. doi:10.1109/WACV48630.2021.00012.
- [8] Y. Chen, J. Shi, C. Mertz, S. Kong, D. Ramanan, Multimodal object detection via bayesian fusion, *CoRR* abs/2104.02904. arXiv:2104.02904.
- [9] M. Sharma, M. Dhanaraj, S. Karnam, D. G. Chachlakis, R. Ptucha, P. P. Markopoulos, E. Saber, Yolors: Object detection in multimodal remote sensing imagery, *IEEE Journal of Selected Topics in Applied Earth Observations and Remote Sensing* 14 (2021) 1497–1508. doi:10.1109/JSTARS.2020.3041316.
- [10] H. Perreault, G. Bilodeau, N. Saunier, M. Héritier, FFAVOD: feature fusion architecture for video object detection, *Pattern Recognition Letter* 151 (2021) 294–301. doi:10.1016/j.patrec.2021.09.002.
- [11] R. Guo, D. Li, Y. Han, Deep multi-scale and multi-modal fusion for 3d object detection, *Pattern Recognition Letter* 151 (2021) 236–242. doi:10.1016/j.patrec.2021.08.028.
- [12] F. Team, et al., Free flir thermal dataset for algorithm training. URL <https://www.flir.com/oem/adas/adas-dataset-form/>

Table 4. Comparison on VEDAI Dataset

Model	Data	Backbone	mAP50	mAP
mono-modality networks				
Retina [27]	RGB	ResNet-50	-	43.5
Faster R-CNN [18]	RGB	ResNet-101	-	34.8
SSSDet [28]	RGB	shallow network	-	46.0
SSD [19]	RGB	VGG16	70.9	-
SSD [19]	IR	VGG16	69.8	-
EfficientDet(D1) [29]	RGB	EfficientNet(B1)	74.0	-
EfficientDet(D1) [29]	IR	EfficientNet(B1)	71.2	-
YOLO-fine [30]	RGB	Darknet53	76.0	-
YOLO-fine [30]	IR	Darknet53	75.2	-
YOLOv5	RGB	CSPDarknet53	74.3	46.2
YOLOv5	IR	CSPDarknet53	74.0	46.2
multi-modality networks				
YOLOv3 early fusion [31]	RGB+IR	Darknet53	-	44.0
YOLOv3 mid fusion [31]	RGB+IR	Darknet53	-	44.6
Baseline(ours)	RGB+IR	CSPDarknet53	79.7	46.8
CFT(ours)	RGB+IR	CFB	85.3	56.0

- [13] X. Jia, C. Zhu, M. Li, W. Tang, W. Zhou, Llvip: A visible-infrared paired dataset for low-light vision, in: Proceedings of the IEEE/CVF International Conference on Computer Vision, 2021, pp. 3496–3504.
- [14] S. Razakarivony, F. Jurie, Vehicle detection in aerial imagery : A small target detection benchmark, Journal of Visual Communication and Image Representation 34 (2016) 187–203. doi:10.1016/j.jvcir.2015.11.002.
- [15] A. Krizhevsky, I. Sutskever, G. E. Hinton, Imagenet classification with deep convolutional neural networks, in: P. L. Bartlett, F. C. N. Pereira, C. J. C. Burges, L. Bottou, K. Q. Weinberger (Eds.), Advances in Neural Information Processing Systems 25: 26th Annual Conference on Neural Information Processing Systems 2012. Proceedings of a meeting held December 3–6, 2012, Lake Tahoe, Nevada, United States, pp. 1106–1114.
- [16] K. He, X. Zhang, S. Ren, J. Sun, Deep residual learning for image recognition, in: 2016 IEEE Conference on Computer Vision and Pattern Recognition, CVPR 2016, Las Vegas, NV, USA, June 27–30, 2016, pp. 770–778. doi:10.1109/CVPR.2016.90.
- [17] R. B. Girshick, J. Donahue, T. Darrell, J. Malik, Rich feature hierarchies for accurate object detection and semantic segmentation, in: 2014 IEEE Conference on Computer Vision and Pattern Recognition, CVPR 2014, Columbus, OH, USA, June 23–28, 2014, pp. 580–587. doi:10.1109/CVPR.2014.81.
- [18] S. Ren, K. He, R. B. Girshick, J. Sun, Faster R-CNN: towards real-time object detection with region proposal networks, IEEE Transactions on Pattern Analysis and Machine Intelligence 39 (6) (2017) 1137–1149. doi:10.1109/TPAMI.2016.2577031.
- [19] W. Liu, D. Anguelov, D. Erhan, C. Szegedy, S. E. Reed, C. Fu, A. C. Berg, SSD: single shot multibox detector, in: B. Leibe, J. Matas, N. Sebe, M. Welling (Eds.), Computer Vision - ECCV 2016 - 14th European Conference, Amsterdam, The Netherlands, October 11–14, 2016, Proceedings, Part I, Vol. 9905, pp. 21–37. doi:10.1007/978-3-319-46448-0_2.
- [20] J. Redmon, S. K. Divvala, R. B. Girshick, A. Farhadi, You only look once: Unified, real-time object detection, in: 2016 IEEE Conference on Computer Vision and Pattern Recognition, CVPR 2016, Las Vegas, NV, USA, June 27–30, 2016, pp. 779–788. doi:10.1109/CVPR.2016.91.
- [21] A. Vaswani, N. Shazeer, N. Parmar, J. Uszkoreit, L. Jones, A. N. Gomez, L. Kaiser, I. Polosukhin, Attention is all you need, in: I. Guyon, U. von Luxburg, S. Bengio, H. M. Wallach, R. Fergus, S. V. N. Vishwanathan, R. Garnett (Eds.), Advances in Neural Information Processing Systems 30: Annual Conference on Neural Information Processing Systems 2017, December 4–9, 2017, Long Beach, CA, USA, pp. 5998–6008.
- [22] J. Wagner, V. Fischer, M. Herman, S. Behnke, Multispectral pedestrian detection using deep fusion convolutional neural networks, in: 24th European Symposium on Artificial Neural Networks, ESANN 2016, Bruges, Belgium, April 27–29, 2016.
- [23] L. Zhang, X. Zhu, X. Chen, X. Yang, Z. Lei, Z. Liu, Weakly aligned cross-modal learning for multispectral pedestrian detection, in: 2019 IEEE/CVF International Conference on Computer Vision, ICCV 2019, Seoul, Korea (South), October 27 - November 2, 2019, pp. 5126–5136. doi:10.1109/ICCV.2019.00523.
- [24] Y. Zheng, I. H. Izzat, S. Ziaee, GFD-SSD: gated fusion double SSD for multispectral pedestrian detection, CoRR abs/1903.06999. arXiv:1903.06999.
- [25] D. Hendrycks, K. Gimpel, Gaussian error linear units (gelus), arXiv preprint arXiv:1606.08415.
- [26] N. Ma, X. Zhang, H. Zheng, J. Sun, Shufflenet V2: practical guidelines for efficient CNN architecture design, in: V. Ferrari, M. Hebert, C. Sminchisescu, Y. Weiss (Eds.), Computer Vision - ECCV 2018 - 15th European Conference, Munich, Germany, September 8–14, 2018, Proceedings, Part XIV, Vol. 11218, pp. 122–138. doi:10.1007/978-3-030-01264-9_8.
- [27] T. Lin, P. Goyal, R. B. Girshick, K. He, P. Dollár, Focal loss for dense object detection, in: IEEE International Conference on Computer Vision, ICCV 2017, Venice, Italy, October 22–29, 2017, pp. 2999–3007. doi:10.1109/ICCV.2017.324.
- [28] M. Mandal, M. Shah, P. Meena, S. K. Vipparthi, SSSDet: simple short and shallow network for resource efficient vehicle detection in aerial scenes, in: 2019 IEEE International Conference on Image Processing, ICIP 2019, Taipei, Taiwan, September 22–25, 2019, pp. 3098–3102. doi:10.1109/ICIP.2019.8803262.
- [29] M. Tan, R. Pang, Q. V. Le, Efficientdet: Scalable and efficient object detection, in: 2020 IEEE/CVF Conference on Computer Vision and Pattern Recognition, CVPR 2020, Seattle, WA, USA, June 13–19, 2020, pp. 10778–10787. doi:10.1109/CVPR42600.2020.01079.
- [30] M. Pham, L. Courtrai, C. Friguet, S. Lefèvre, A. Baussard, Yolo-fine: One-stage detector of small objects under various backgrounds in remote sensing images, Remote Sensing 12 (15) (2020) 2501. doi:10.3390/rs12152501.
- [31] M. Dhanaraj, M. Sharma, T. Sarkar, S. Karnam, D. G. Chachlakis, R. Ptucha, P. P. Markopoulos, E. Saber, Vehicle detection from multi-modal aerial imagery using YOLOv3 with mid-level fusion, in: F. Ahmad (Ed.), Big Data II: Learning, Analytics, and Applications, Vol. 11395, 2020, pp. 22 – 32. doi:10.1117/12.2558115.